# 3D Printed Porous Media Columns with Fine Control of Column Packing Geometry

Conan Fee*, Suhas Nawada, Simone Dimartino

Department of Chemical & Process Engineering and Biomolecular Interaction Centre, University of Canterbury, Private Bag 4800, Christchurch 8020, New Zealand

*Corresponding Author:
Email: conan.fee@canterbury.ac.nz
Phone: +64 3 364 2139
Fax: +64 364 2063

**Abstract**

In this paper we demonstrate, for the first time, the use of 3D printing (also known as additive manufacturing or rapid prototyping) to create porous media with precisely defined packing geometries, directly from computer aided design (CAD) models. We used CAD to design perfectly ordered beds with octahedral beads (115 μm apothem) packed in a simple cubic configuration and monoliths with hexagonal channels (150 μm apothem) in parallel and herringbone arrangements. The models were then printed by UV curing of acrylonitrile-butadiene-styrene powder layers. Each porous bed was printed at 1.0, 1.5 and 2.0 mL volumes, within a complete column, including internal flow distributors and threaded 10-32 flow connectors. Close replication of CAD models was achieved. The resultant individual octahedral beads were highly uniform in size, with apothems of 113.6 ± 1.9 μm, while the monolith hexagonal cross-section channels had apothems of 148.2 ± 2.0 μm. Residence time distribution measurements show that the beds largely behaved as expected from their design void volumes. Radial and fractal flow distributor designs were also tested. The former displayed poor flow distribution in parallel and herringbone pore columns, while the fractal distributors provided uniform flow distribution over the entire cross section. The

results show that 3D printing is a feasible method for producing precisely controlled porous media. We expect our approach to revolutionize not only fundamental studies of flow in porous media but methods of chromatography column production.

**Keywords:** Porous media; 3D printing; Additive manufacturing; Packed bed; Packing geometry; Residence time distribution

## Introduction

Porous media are important for fluid-solid contacting in many unit operations, including adsorption, chromatography, catalysis and filtration. Media particles are typically packed into a column, allowing fluid to flow through the interstitial voids, thus bringing the fluid into close contact with the solid phase. Key to the effectiveness of packed columns are the flow-related properties of mass transfer, fluid distribution, back pressure and fluid dispersion, which in turn depend upon packing geometry.

Packing geometry is determined primarily by particle shape, size and size distribution and the packing method used. While there have been many theoretical studies on optimal packing configurations and their effects on packing density, along with computational studies on theoretical plate height and flow dispersion (e.g. [1]), packed beds have, for practical reasons, invariably been randomly packed to date. Thus, there has been no way before now to translate optimal ordered packing arrangements into practice.

There have been many studies on flow through randomly packed beds, notably the seminal works of Darcy [2], Kozeny [3], Carman [4] and Ergun [5]. These and other authors have contributed much to our understanding of pressure drop and fluid dispersion as functions of flow rate, particle shape, size and size distribution, largely based upon empirical characterization. Experimental replication of models with specific random or ordered packing geometries has been challenging. For random geometries, no two randomly packed beds are exactly alike so we rely upon generalized correlations and efficiency factors where, to quote Khirevich et al. [6]: "column packing and consolidation are largely treated phenomenologically and considered an art rather than a science". On the other hand, it has been impracticable to precisely reproduce ordered packing at the micron scale, mainly because there has been no practical way to precisely locate individual particles within a bed. Even if precise placement of the particles were feasible, e.g. through manual placement of each bead, the column walls would almost certainly frustrate attempts to maintain order.

Some authors (e.g. [7-10]) have characterized existing randomly packed beds through tomography, thus reproducing, *a posteriori*, the geometry of their experimental columns for computational analysis. However, they have had no control over the initial packing of the experimental beds at the individual particle level so it has been a case of accepting, rather than *a priori* designing, the fine structural detail. Furthermore, because individual particles may change their positions with time, the characterization of packing geometries is valid only as a snapshot in time.

Efforts to optimize the performance of packed beds for chromatography have focused on the manufacture of bed particles (resin) and, because of ease of manufacture and guaranteed bed permeability, these have been predominantly spherical [11]. Many methods have been developed for producing spherical beads in bulk but they typically result in wide particle size distributions, which are minimized in final media products by fractionation, leading to increased costs, inefficient production and ultimately variations in packing geometry through size variation in all but the most expensive of media.

In this paper, we introduce an entirely new approach to packed column manufacture that solves many of the above problems, using 3D printing (also known as "additive manufacturing" or "rapid prototyping") to produce packed beds that precisely replicate computer aided design (CAD) models. 3D printing is a generic term for techniques by which solid objects are created from digital models. The first working 3D printer was patented by Hull with a priority date of 1984 [12]. Since then, a variety of 3D printing systems have been developed, including fused deposition, selective heat or laser sintering, photopolymerization and thin-film lamination. Several recent reviews of the development and advances in 3D printing are available [13-17].

We use the term "packed" above advisedly because our technique produces what might better be described as monoliths, although, as described below, they are distinct from monoliths in their current sense in chromatography, which effectively exchange random particle packing for random pore geometries [18, 19]. In contrast, with our approach, we have created and tested exact physical replicas of ordered packed bed CAD models, comprising ordered arrays of uniform particles. Our approach opens up the possibility, for the first time, to precisely locate and orient every individual particle within a porous bed. Here, we also demonstrate the production of monoliths with precise internal pore geometries and, moreover, show that we can print not only the porous bed but the entire column, complete with internal flow distributors, packing, and external fluid connectors, therefore creating single-piece chromatography columns.

## Materials and Methods

Stereolithography (STL) files for the column models were created on Solidworks 2012 (Dassault Systèmes, Paris, France) and printed on a 3DS Projet HD 3500 printer (3D Systems, Rock Hill, SC, USA). The printed components were made from non-porous urethane acrylate oligomers (acrylonitrile butadiene styrene, ABS). A proprietary paraffin wax was also used by the 3D printer during printing to support overhanging features. The wax was removed from the internal structures of the columns by alternating warm water (70°C) and 100% cyclohexane washes for up to 3 h.

The CAD models included the “packed” porous core and the ancillary column elements, namely column walls, fluid distributors and collectors and end fittings for easy connection to the experimental chromatography system. This enabled our “packed” columns to be printed as an all-in-one parts, with no further assembly required before use.

The porous beds were created with three geometries: beads in a simple cubic arrangement (SC, Fig. 1a), a monolith containing parallel channels (PC,  Fig. 1b) and another containing herringbone shaped channels (HC,  Fig. 1c).

The nominal resolution of the 3D printer was 28 μm, but the limiting dimensions of the lattice elements that could be reliably printed at the desired resolution were about one order of magnitude larger. Polyhedrons and polygons were used to design the "packing" elements rather than spheres and circles, to minimize the file size of the STL models while maintaining a regular shape in the lattice elements. For this reason, octahedral beads (115 μm apothem) were used in the SC arrangement, while channels with hexagonal cross-sections (150 μm apothem) were used for both the PC and HC configurations. The HC geometry was designed with a tortuosity of 1.15, where the tortuosity is defined as the ratio between the total length of the channels and the column height.

In a standard SC configuration, only the outer diameters of the beads would contact, creating a relatively weak structure prone to movement of the individual beads. The octahedral beads were therefore designed to overlap at the edges (Fig. 1a), ensuring the manufacture of physically robust prototypes with particle positions that do not change with time. An overlap factor, defined as the ratio between the distance between the centers of two adjacent polygons and the external bead face-to-face diameter, was applied. Initial experiments indicated that an overlap value of 1.4 would yield a physically robust monolithic structure.

Columns with total bed volumes of 1, 1.5 and 2 ml were produced for each packed bed geometry studied. The internal diameter and wall thickness of the cylindrical columns were 16 and 2 mm, respectively. Connection with the chromatography system was facilitated by including a 10-32 standard coned, female, fast protein liquid chromatography (FPLC) finger-tight fitting at each end of the columns. All columns contained a flow distributor at the porous bed entrance and an identical flow collector at the outlet. Two geometric designs for the flow distributor and collector were used, a standard radial distributor comprising a set of concentric and radial channels, and a fractal flow distributor with square cross-section and 1024 nodes as proposed by Tondeur and Luo [20]. The corresponding printed columns, therefore, were of circular and square cross-sections, accordingly to the flow distributor considered. Figure 2 presents solid models of the flow channels within each distributor (collector) design, which were then subtracted from the solid ends of the columns in the CAD model to produce the flow channels. The characteristics of the 3D printed columns are summarized in Table 1.

Residence time distribution (RTD) tests were carried out using an ÄKTA explorer 10™ FPLC system equipped with an auto-sampler (GE Healthcare, Uppsala, Sweden). The columns were first equilibrated with pure water for 15 column volumes (CV), followed by injection of 30 µl of 2 M NaCl. RTD experiments were carried out at a flow rate of 10 ml/min, which corresponds to superficial velocities of 298 and 295 cm/h for the circular and square cross-section columns, respectively. The conductivity peak in the column effluent was recorded and analyzed using the moment method. The injected volume was 6% or less of the void volumes of the columns tested, hence the contribution to the first moment arising from the injection loop can be neglected. Under this assumption, the experimental residence time, $t_r^{\exp}$, can be calculated as:

$$t_r^{\exp} = \frac{M_1}{M_0} = \frac{\int_0^\infty c(t)t\,dt}{\int_0^\infty c(t)\,dt} \qquad (1)$$

where $M_i$ is the i$^{th}$ absolute moment, $c$ is the concentration of the tracer, and $t$ is time. E curves, i.e. normalized elution profiles having unitary area, were calculated from the conductivity signal and the 0$^{th}$ moment:

$$E(\theta) = \frac{c(\theta)}{M_0} \qquad (2)$$

where $\theta$ is the dimensionless time defined in terms of the theoretical residence time, $t_r^{theo}$, estimated from the designed geometry of the lattice structure:

$$\theta = \frac{t}{t_r^{theo}} \qquad (3)$$

This expression can be also used to define an experimental dimensionless residence time, $\theta_r^{\exp}$:

$$\theta_r^{\exp} = \frac{t_r^{\exp}}{t_r^{theo}} \qquad (4)$$

Comparison of the theoretical and experimental residence times was used to assess the quality of the printed lattices and the uniformity of the flow distribution.

## Results and Discussion

Creation of STL models represents the first step in the production of the 3D printed porous columns. Definition of the building elements of the lattice is crucial, in part because this is the attribute that has the most influence on file size and subsequent file handling. Contribution to the final file size arising from column walls, end fittings, and distributor/collector can be neglected. In the initial design, spherical beads and circular channels were considered but the STL file sizes were too large, from both the viewpoints of the speed of rendering during CAD modeling and of the printer file handling capacity. For example, to accurately model a single sphere, irrespective of diameter, our CAD package used approximately 6162 triangles, with a file size of 306 kbytes, while an octahedron was described by only 8 triangles, giving a file size of less than 0.5 kbytes, three orders of magnitude smaller. However, file size *per se* is not fundamentally a limiting factor for 3D printing, and could be handled with efficient computational algorithms or compression, particularly with the constantly growing capacity of microprocessors, communications and storage media with time. Furthermore, ordered packing geometries are based on repetitive structures that would lend themselves to iterative printer command sequences. Thus, there is no fundamental reason why spherical elements could not be used, given sufficient software and hardware processing power.

It is well understood that in 2D image processing, the resolution of a picture is proportional to the number of pixels of which it is comprised. Similarly, the quality of the rendering of a solid shape is proportional to the number of 3D dots used to discretize it. The resolution of a 3D printer is an indication of the size of the smallest feature that is possible to print, i.e. it corresponds to the dimensions of the “3D dots” that make up the printed model. However, the final size and shape of the 3D dots are ultimately determined by a number of uncontrollable variables. In our case, using layer deposition followed by UV curing, examples of these uncontrollable variables are: i) the interfacial forces acting between the ABS polymer and the support material, ii) the local temperature of the ABS polymer during UV curing, iii) venting characteristics of the printing chamber, iv) defects and irregularities during layering of the ABS powder.

Also, the resolution quoted by a 3D printer manufacturer may well comprise the best possible that can be achieved under ideal conditions but this may not be routinely achievable in normal practice. The 3D printer used in this work had a nominal resolution of 28 μm so the printed octahedral particles or hexagonal cross-section channels were characterized by relatively rounded edges at the micron scale. However, as is shown in the following discussion, the features of the CAD models were conserved in the 3D printed objects, hence microscopic limitations in the resolution do not represent a significant limitation of 3D printed porous media.

In addition to full operational columns, cross-sectional "cutaway" models of each packing configuration were printed to display the internal structures of the columns, distributors and porous beds. Figure 3 shows that not only the column macrostructures but also the microstructures of the CAD models were reproduced with reasonable fidelity by the printer.

Inspection of Fig. 3 reveals that the mean bead and channel apothems were 113.6 ± 3.8 and 148.2 ± 2.0 μm, respectively, while the design values were 115 and 150 μm, respectively, demonstrating the precise control over packed bed microstructures delivered by our 3D printing approach. Figure 3c shows a magnification of the simple cubic cutaway model, showing that the particles were approximately octahedral and the dimensions of the pores and relative diameters of the beads were consistent with the design compression factor $\alpha = 1.4$. Likewise, magnified images of the straight and herringbone channels (Fig. 3f and 3l) show reasonable fidelity between the CAD models and the printed columns in the cutaway models, revealing that the 3D printer used was able to reproduce the CAD models well. It is reasonable to expect the same fidelity was obtained between the CAD models and the full operational printed columns.

Residence time distribution (RTD) tests were conducted on all 3D printed columns, first, to highlight differences between the "packing" geometries used and, second, to compare the effectiveness of the two distributor designs.

Normalized residence time distribution profiles of the printed columns are shown in Fig. 4. We were concerned that the printer might not faithfully reproduce octahedral beads but rather create roughly spherical beads because of limitations in resolution. However, evidence of the high fidelity between the CAD model and the 3D printed columns can be found in the RTD experiments by comparing theoretical and experimental porosity values. At α = 1.4, the designed extra-particle porosity of the simple cubic octahedral beads is ε = 0.575. For comparison, a simple cubic configuration of spherical beads with the same overlap would have a theoretical porosity of ε = 0.041, while it would be ε = 0.476 with no overlap. The experimentally determined porosities of ε = 0.678, 0.569 and 0.551 for 1, 1.5 and 2 ml columns are closer to the design porosity for octahedral beads (17.9%, 1.0% and 4.2% differences, respectively) rather than that for spherical particles (minimum difference 34.4%), suggesting good control over particle shape at the 3D printer's limiting resolution. The mean normalized residence times for simple cubic bead columns also indicate reasonable consistency between the design (expected) and experimental column porosities.

The low mean residence times in the straight and herringbone channel cylindrical columns (Fig. 4a) compared with the cubic packing suggest that a substantial proportion of the channels in those columns were not accessed by the fluid when using radial flow distributors. This is a strong indication of the low efficiency of the radial distributor, which was not able to spread the incoming flow uniformly over the entire cross section. The radial distributor primarily conveys the flow through the central channel, while there is no reason for flow to move radially in the distributor unless there is an axial flow resistance in the bed. In the case of cubic packing, the interconnected network of beads allows for both radial and axial dispersion, so it is the packing itself that assists in the uniform distribution of the flow across the cross-section, giving an experimental dimensionless residence time, $\theta_r^{exp}$, close to unity (Fig. 4 and Table 2). In contrast, because radial dispersion is absent throughout the parallel and herringbone channel columns, the fluid would have followed only the channels into which it initially entered. It is likely, therefore that the performance of these latter columns was limited by inadequate radial flow distribution at entry, resulting in $\theta_r^{exp} < 1.0$ in the RTDs shown in Figure 4a.

In an attempt to improve uniform flow distribution over the entire cross-section, a fractal distributor was designed. For both the radial (circular column cross-section) and fractal (square column cross-section) designs, we printed shortened columns containing no bed but with the inlet flow distributor and outlet flow collector placed immediately adjacent to one another and compared their residence time distributions. This approach may also be useful to measure extra-bed dispersion but in this case we simply compared the average residence times of the two distributor designs. The mean residence times for the radial and fractal distributors were $\theta_r^{exp} = 0.32$ and 0.93, respectively, indicating that flow was not well distributed in the radial flow distributor, while it was relatively uniformly distributed in the fractal design.

Figure 5 compares the normalized RTD curves in 2 ml PC (Fig. 5a) and SC (Fig. 5b) columns containing the two distributor designs. Note that there is a significant difference between the mean elution times for the two distributor designs in the PC column, in which there was no radial dispersion within the bed itself, while in the simple cubic bead column, where the bed itself provides radial distribution, there was little difference between the RTDs for the two distributor designs. Thus, for bed pore geometries that do not promote radial flow dispersion, careful design of the fluid distributor is required.

Note also, in Fig. 5b, that the fractal distributor system for the SC column resulted in a longer tailing in the RTD curve. This possibly occurs because the flow rate in the corners of the square cross-section column with the fractal distributor may be slower for the SC packing than the mean flow rates in the rest of the bed, leading to greater axial dispersion than that in the cylindrical cross-section column. These differences in tailing are not seen between the two PC columns (Fig. 5a) because the axial dispersion is affected only by the flow through the independent channels, which have uniform geometry, regardless of the overall column cross-sectional geometry.

Pressure-flow measurements of the printed columns were found to be indistinguishable from control measurements using just the FPLC system in by-pass mode (i.e. with no column attached, data not shown). This result is consistent with expectations because short columns were used, resulting in low column backpressures. No external structural defects nor leaks were observed at superficial velocities of up to 594 $cm.hr^{-1}$ (corresponding to 20 $ml.min^{-1}$), demonstrating the structural robustness of the all-in-one-piece 3D printed columns.

Our choice of materials for this work was constrained to those that were readily available for rapid prototyping, so we used a non-porous material and focused on demonstrating that we could achieve control over packing geometry, at least within the resolution of the particular printer used here. Clearly, an ideal chromatographic media would comprise finer-resolution elements to minimize the theoretical plate height, a functionalizable surface chemistry to enable ligand attachment for reversible adsorption, and porous materials to maximize adsorption capacity. We have not demonstrated these ideal characteristics in this paper but see no fundamental reasons why all of these ideal characteristics could not be achieved. We also limited the volumes of our columns to those that were convenient to handle in the laboratory. However, even with the printer used here, there is no particular reason why we could not have produced columns with significantly greater dimensions, at the same fine resolution but with a diameter and length of 30 cm or more i.e. preparative scale. The materials used here were low-cost and in general, the use of materials in 3D printing is very efficient, using only the amount necessary to produce the specific features of the CAD model. Thus, we believe our approach is scalable and will enable not only fundamental studies of flow, mass transfer and adsorption through structured porous media but perhaps, in time, commercial column production.

Our approach can be applied not only to chromatography but to any application requiring fluid-solid contacting, including filtration and catalytic or other reaction applications. One could create precise replicates of randomly packed beds, to enable experimental validation of computational models. Furthermore, the ability to orientate the individual particles means we can go beyond using spheres and conceive beds comprising unusual and complex particle shapes, while maintaining uniform porosity throughout. There is no particular need for all elements within the bed to be uniform with regard to size or shape and one could imagine porous media with a wide range of controlled geometry elements throughout the bed could be designed and printed. There are currently printers on the market capable of printing multiple materials at once (rather like a color inkjet printer) so the various column and bed components could, in principle, be printed using different materials, each suited to its particular purpose e.g. porous, functional bed materials with non-porous, inert column walls, flow connectors and distributors.

Thus, there is enormous potential for using additive manufacturing to produce versatile monolithic porous media with designed geometries not only for the beds themselves but for the entire columns.

## Conclusions

We have shown, for the first time, that 3D printing can be used to precisely replicate the fine structure of CAD models of porous media, comprising both ordered particle packing and monoliths with internal channels. Residence time distributions measured in the printed columns were consistent with predicted porosities and designed geometric structures, indicating that the CAD features were reproduced with good fidelity at the scales attempted here.

Furthermore, we have demonstrated that not only the porous beds themselves but entire columns can be printed as single physical artifacts, meaning that flow connectors, flow distributors and internal column packing can be printed within a single, complete column. Fractal flow distributors are capable of distributing the flow across the entire column cross-section, even when there is no radial dispersion across the flow channels of monolithic beds. This distributor design enabled the creation of square cross-section monolithic columns with good flow distribution and residence time distributions through parallel channels that were independent of the column cross-sectional shape.

3D printing frees us from the constraints of previous manufacturing methods and enables the creation of porous media characterized by a combination of fine precision, scalability and versatility, at low cost. We expect this approach to column design will revolutionize the production of packed bed columns and monoliths across a wide range of applications, not only in chromatography but also filtration, catalysis, adsorption and other applications where intimate fluid-solid contact is desired.

**Acknowledgement**

S. Nawada gratefully acknowledges a PhD scholarship from the Biomolecular Interaction Centre, University of Canterbury. This work was partially funded by a Ministry of Business, Innovation and Employment Smart Ideas Grant UOCX1304.

## References

1. M.R. Schure, R.S. Maier, J. Chrom. A 1126(1-2) (2006) 58.
2. H. Darcy, Les Fontaines Publiques de la Vile de Dijon, Victor Dalmont, Paris, 1856.
3. J. Kozeny, Sitzungsber Akad. Wiss 136(2a) (1927) 271.
4. P.C. Carman, Trans. Inst. Chem. Eng. Lond. 15 (1937) 150.
5. S. Ergun, Chem. Eng. Prog. 48(2) (1952) 89.
6. S. Khirevich, A. Daneyko, A. Höltzel, A. Seidel-Morgenstern, U. Tallarek, J. Chrom. A 1217(28) (2010) 4713.
7. A. Akolkar, J. Petrasch, Transp. Porous Media 95(3) (2012) 535.
8. Y.X. Cao, B. Chakrabortty, G.C. Barker, A. Mehta, Y.J.Wang, Europhys. Lett. 102(2) (2013) 24004-p1.
9. R. Moreno-Atanasio, R.A. Williams, X.D. Jia, Particuology 8(2) (2010) 81.
10. M. Schubert, A. Bieberle, F. Barthel, S. Boden, U. Hampel, Chem. Ing. Tech. 83(7) (2011) 979.
11. M.T. Gokmen, F.E. Du Prez, Prog. Polym. Sci. 37(3) (2012) 365.
12. C. W. Hull, US Patent 4575330 (1986).
13. D.H. Freedman, Technol. Rev. 115(1) (2012) 50.
14. R.D. Goodridge, C.J. Tuck, R.J.M. Hague, Progr. Mat. Sci. 57(2) (2012) 229.
15. D.D. Gu, W. Meiners, K. Wissenbach, R. Porawe, Int. Mat. Rev. 57(3) (2012) 133.
16. S. Kumar, J.P. Kruth, Mater. Des. 31(2) (2010) 850.
17. Wendel, B., et al., *Additive Processing of Polymers.* Macromolecular Materials and Engineering, 2008. **293**(10): p. 799-809.
18. A. Nordborg, E.F. Hilder, Anal. Bioanal. Chem. 394(1) (2009) 71.
19. Z. Walsh, B. Paull, M. Macka, Anal. Chim. Acta 750 (2012) 28.
20. D. Tondeur, L.G. Luo, Chem. Eng. Sci. 59(8-9) (2004) 1799.

## Figure Legends

**Figure 1.** The three bed geometric designs: a) simple cubic beads, b) straight channels, c) herringbone channels

**Figure 2.** Illustration of the flow distributor templates: a) radial flow distributor, b) fractal flow distributor (Note: for clarity, only the first 64 of the 1024 nodes are shown)

**Figure 3.** CAD designs versus printed cutaway columns a) SC CAD model b) SC printed model c) 20X magnification of SC beads d) PC CAD model e) PC printed model f) 20X magnification of parallel channels g) HC CAD model h) HC printed model l) 20X magnification of herringbone channels

**Figure 4.** Residence time distribution profiles of a) the three packing geometries in 1.5 ml cylindrical columns, b) SC bead columns at three different column volumes.

**Figure 5.** Comparison of 2 ml columns with radial and fractal flow distributors for a) PC columns b) SC columns

**Table 1.** Specifications of 3D Columns

| Column Cross-Section | Flow Distributor | Column Volumes (ml) | Packing Configuration | Theoretical Porosity |
|---|---|---|---|---|
| Circular | Radial | 1.0, 1.5, 2.0 | SC | 0.575 |
| Circular | Radial | 1.0, 1.5, 2.0 | PC | 0.334 |
| Circular | Radial | 1.0, 1.5, 2.0 | HC | 0.334 |
| Square | Fractal | 2.0 | SC | 0.575 |
| Square | Fractal | 2.0 | PC | 0.393 |

**Table 2.** Theoretical and experimental mean residence times of SC columns

| Column Volume (ml) | $t_r^{theo}$ (min) | $t_r^{exp}$ (min) | $\theta_r^{exp}$ (-) |
|---|---|---|---|
| 1.0 | 0.705 | 0.804 | 1.14 |
| 1.5 | 0.993 | 0.993 | 1.00 |
| 2.0 | 1.280 | 1.229 | 0.96 |

**Figure 1**

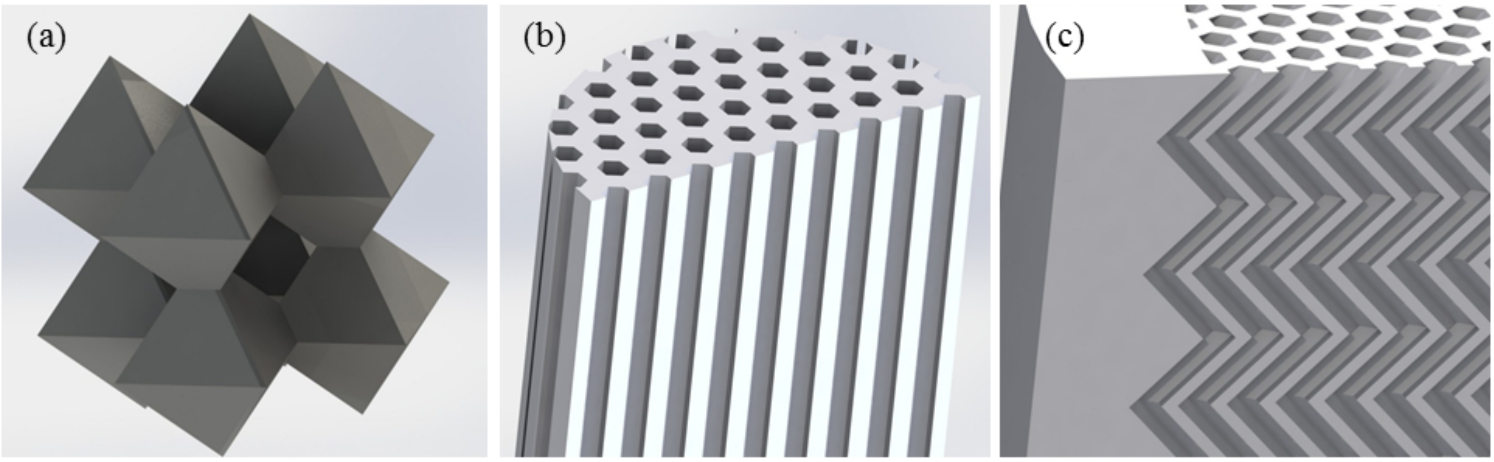

**Figure 2**

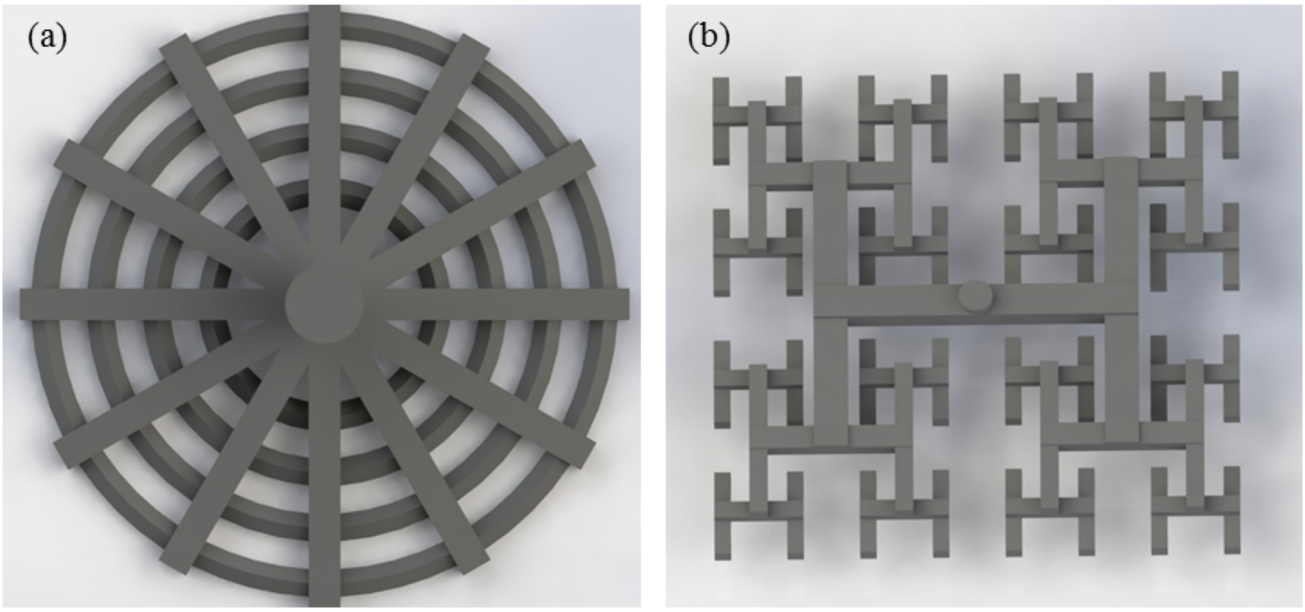

**Figure 3**

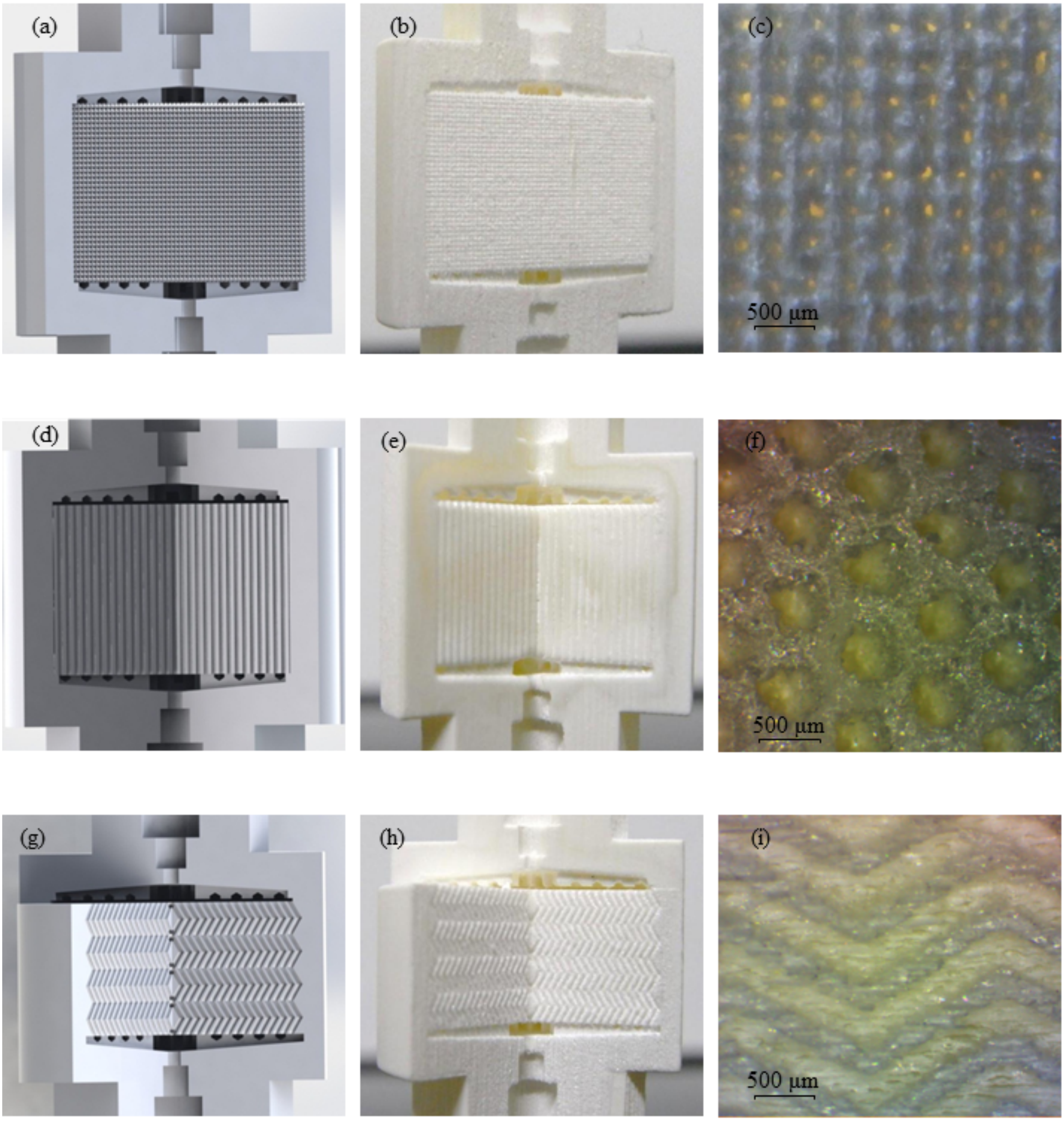

**Figure 4**

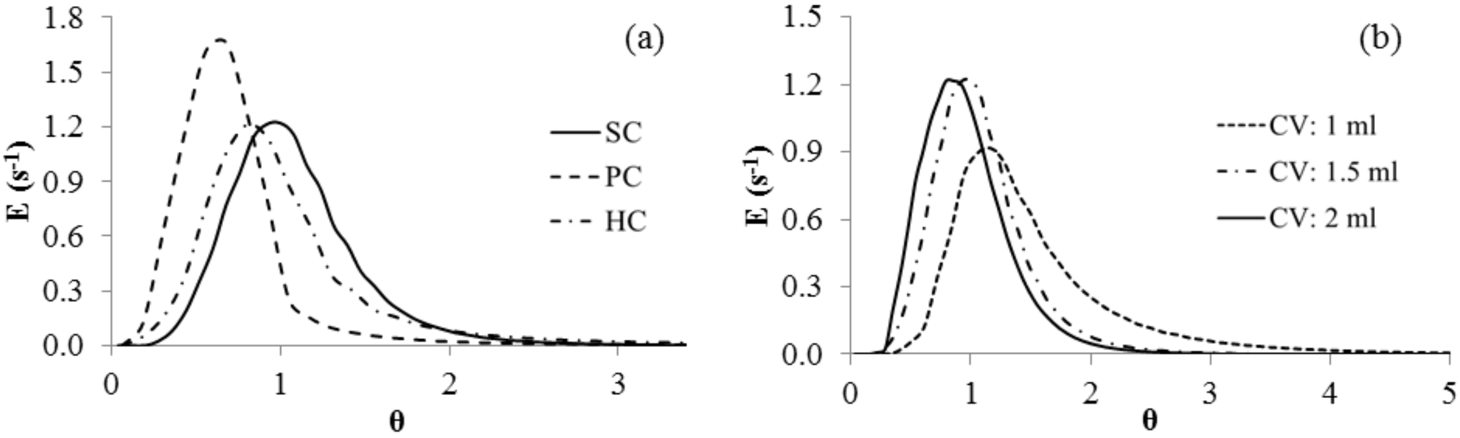

1.8
1.5
1.2
0.9
0.6
0.3
0.0
E (s-1)
(a)
SC
PC
HC
0
1
2
3
θ
1.5
1.2
0.9
0.6
0.3
0.0
E (s-1)
(b)
CV: 1 ml
CV: 1.5 ml
CV: 2 ml
0
1
2
3
4
5
θ

**Figure 5**

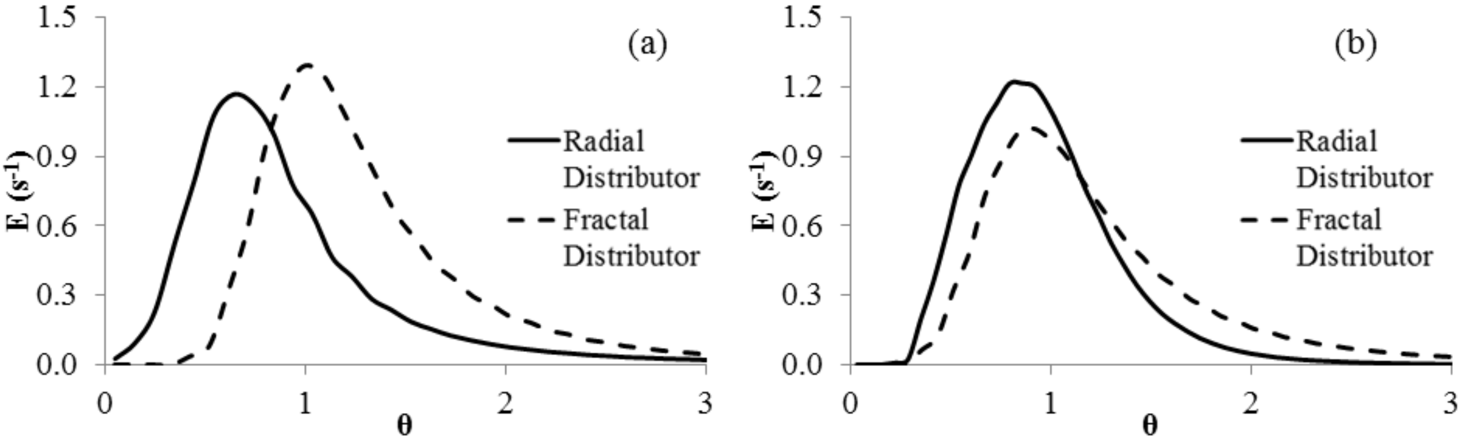
1.5
1.2
0.9
0.6
0.3
0.0
0
1
2
3
E (s-1)
θ
(a)
Radial Distributor
Fractal Distributor
(b)
Radial Distributor
Fractal Distributor